Thermodynamics for clay minerals: Calculation tools and application to the case of illite/smectite interstratified minerals

Philippe Blanc, F. Gherardi, P. Vieillard, Nicolas C.M. Marty, Hélène Gailhanou, Stéphane Gaboreau, Bruno Letat, C. Geloni, E.C. Gaucher, Benoît Made

Thermodynamics for clay minerals: calculation tools and application to the case of illite/smectite interstratified minerals

P. Blanc[1*], *Gherardi F.*[2], *Vieillard P.*[3], *Marty N.C.M.*[1], *Gailhanou H.*[1], *Gaboreau S.*[1], *Letat B.*[1], *Geloni C.*[4], *Gaucher E.C.*[5], *Madé B.*[6]

[1]BRGM, 3 Avenue Claude Guillemin, 45060 Orléans Cedex 2, France
[2]IGG – CNR, Via G. Moruzzi, 56124 Pisa, Italy
[3]CNRS-IC2MP-UMR-7285 Hydrasa, 5 av. Albert Turpain, 86073 Poitiers Cedex, France
[4]Geological Laboratories, ENI S.p.A., San Donato Milanese, Italy.
[5]TOTAL S.A., Avenue Larribau, 64018 Pau, France
[6]ANDRA, 92298 Châtenay-Malabry, France.
* Corresponding author : p.blanc@brgm.fr

Abstract

We present two computing tools, ClayTherm and ISTherm, devoted to the estimation of the thermodynamic properties of both anhydrous and hydrated clay minerals (ClayTherm), and of illite/smectite (I/S) mineral series (ISTherm). The first computing tool, ClayTherm, is devoted to thermodynamic property estimates for clay minerals. It combines several previously published estimation models, including hydration aspects. Verification is provided, against a set of solubility data, selected from previous literature. A specific application ISTherm was subsequently developed based on the first tool. It focuses on the smectite-to-illite transformation, and is able to calculate the thermodynamic properties of a series of illite/smectite (I/S) interstratified minerals, starting from the composition of a single I/S sample. The thermodynamic functions have been completed for the mixing energies and the tool was then used in order to investigate the case of a natural I/S hydrothermal series from the Shinzan geothermal field (Japan). Activity diagrams have been calculated including illite/smectite and phase relations are found to be in agreement with previous mineralogical observations and solution chemical analyses. The I/S series from Shinzan is further investigated through reactive transport modelling by using a site-specific, augmented version of the geochemical database. Illitization through the formation of I/S is predicted over realistic reaction times, consistently with available mineralogical observations.

Keywords: Thermodynamics, clay minerals, interstratified illite/smectite, environment

1. Introduction

Knowledge of the thermodynamic properties of clay minerals is essential for the prediction of the chemical behaviour of clayrock, soils or artificial materials (engineered barriers, additives, drugs, etc.) in various sub-surface geological systems (Velde, 1992). Such knowledge is needed to precisely model the chemical composition of clayrock porewaters (Gaucher et al., 2009) or the interactions between engineered clay barriers and concrete (Marty et al., 2009) in the context of deep disposal of radioactive waste. In the nuclear waste management context, clay minerals are considered as good candidates for waste confinement barriers due to their low permeability, high plasticity and adsorption properties (Landais, 2006). This is especially the case of materials containing large amounts of smectites. In order to assess the stability of barrier concepts over long periods of time (more than 100,000 years), geochemical modelling is a valuable tool for predicting mineralogical and chemical evolutions. Thermodynamic properties are essential for such applications but they are still poorly understood for clay minerals, with little unambiguous experimental data available. This work first presents the development of a computing tool, combining several previously published estimation models, including 7, 14 and 10Å phases, and, for the latter, offering the capacity to hydrate in contact with aqueous solution.

Illite/smectite mixed layer clay minerals (I/S) are widely present in the natural environment and occur in various contexts, notably during diagenetic processes in sedimentary basins (Hower and Mowatt, 1966), or hydrothermal alteration of volcanic rocks (Inoue, 1983). Understanding the processes associated with the transformation of smectite into illite/smectite and its consequences on mechanical and geochemical behaviour for clay formation is of great importance in some major application fields, such as oil exploration (Geloni et al., 2017) or nuclear waste disposal (Meunier et al., 1998), CO_2 storage in underground reservoirs (Gherardi and Audigane, 2014; Wertz et al., 2013) or for geothermal field exploration (Battaglia et al., 2013). For instance, smectite-to-illite conversion reactions may generate overpressure in sedimentary basins due to the dehydration of smectite that can be problematic for oil well production (Tremosa et al., 2020). Based on the chemical analyses of natural I/S samples, Meunier and Velde (1989) described interstratified illite/smectite using a ternary composition model (one illite and two montmorillonite end-members). Based on this approach, Blanc et al. (1997) developed a solid solution model allowing the calculation of the energies of mixing of illite and smectite layers depending on the degree of order of the stacking sequences.

This work brings the opportunity to develop a specific calculation tool able to determine the composition of these end-members based on the composition of a single I/S sample. The tool itself corresponds to an evolution of a previous development proposed by Geloni et al. (2017), implementing intermediate composition calculations. For the thermodynamic calculation, the tool systematizes the approach proposed previously by Gailhanou et al. (2019), including an assessment of the non-ideal mixing energies. The method is illustrated using a previously documented case of hydrothermal smectite illitization, i.e. the Shinzan area series (Inoue and Utada, 1983).

2. Previous advances and context

Until now, much of the available thermodynamic data for clay minerals have been derived either from solution experiments or from predictive calculations. Numerous experimental studies of equilibration in solution have been conducted since the pioneering work of Reesman and Keller (1968). Equilibration experiments on illite were repeated by Kittrick (1984) and Aja et al. (1991). The case of smectite was investigated, among others, by Reesman and Keller (1968), May et al. (1986), and Kittrick and Peryea (1988). Essene and Peacor (1995) criticised the solution experiments and the properties derived from these studies have not been included so far in the usual thermodynamic databases for geochemical modelling. To overcome such issues, calorimetric measurements have been carried out in the last decade, on a variety of clay minerals, following methods which are described in detail by Gailhanou et al. (2007, 2009, 2012 and 2013) and Blanc et al. (2014). A compilation of the measured thermodynamic properties is provided by Blanc et al. (2015). Recently, Gaboreau et al. (2020) showed, for four clay mineral samples, that solution experiments could provide thermodynamic properties close to calorimetric measurements. This result was achieved under the following conditions: (i) equilibration experiments lasting at least two (2) years, and (ii) reaction temperature increasing from 25 to 40°C, to enhance equilibration kinetics. Note that both calorimetry and solubility experiments were performed on the same samples.

For decades, estimation methods (Chermak and Rimstidt, 1989; Van Hinsberg et al., 2005a, b; Vieillard, 2000, 2002) remained the usual source of thermodynamic data for clay minerals, although neither parametrization nor verification could be assessed against the thermodynamic properties of actual clay minerals. Blanc et al. (2015) proposed a model, based on Vieillard and Tardy (1988), Vieillard (1994a), Vieillard (1994b) and on Chermak and Rimstidt (1989) formalisms to estimate the whole set of thermodynamic properties ($\Delta_f H^0$, S^0, $Cp^0(T)$ and even V^0). The model was parameterized and verified, on the basis of properties extracted from calorimetric measurements performed on actual clay minerals. Unfortunately, the model by Blanc et al. (2015) only applies to anhydrous phases, and it cannot be verified with respect to the experimental data and the compilation of solubility constants recently provided by Gaboreau et al. (2020).

To overcome this difficulty, H_2O vapour isotherms were measured by Gailhanou et al. (2017) and Vieillard et al. (2019), and the results were gathered to develop a hydration model able to predict thermodynamic properties of hydration over a large range of clay mineral compositions. Combining the approaches developed by Blanc et al. (2015), Gailhanou et al. (2017) and Vieillard et al. (2019) would allow the prediction capacities to be tested with respect to solubility data obtained or selected by Gaboreau et al. (2020). A similar approach was proposed by Vidal and Dubacq (2009) and Dubacq et al. (2010). In our case, parameterization and verification are performed based on thermodynamic properties measured specifically on clay minerals. The model developed by Vidal and Dubacq (2009) and Dubacq et al. (2010) is based on Chermak and Rimstidt (1989) work, for the anhydrous part. This latter work had been improved in a version specifically devoted to clay minerals by Blanc et al. (2015), providing estimates more accurate for this specific group of minerals.

The approaches developed by Blanc et al. (2015), Gailhanou et al. (2017) and Vieillard et al. (2019) can be combined according to the workflow displayed in Figure 1. Ultimately, it allows equilibrium constants to be predicted for clay minerals and a comparison of the calculated thermodynamic properties to be made with respect to solubility data selected from the literature.

3. Theoretical background

Classic thermodynamic relations and conventions theoretically apply to clay minerals as with any other mineral. Consequently, the formation properties of a clay mineral will depend on the definition of a reference state. The reference state is considered as the standard state, at 1 bar and 298.15K. Following Helgeson et al. (1978), the pressure between the temperature interval 273.15 to 373.15K is constant, at 1 bar. For T > 373.15K (100°C), the pressure is obtained from the water liquid-vapour curve. Considering a phase AB, its apparent Gibbs free energy of formation $\Delta_a G^0_{AB,P,T}$ is given, at P and T, by the relation:

$$\Delta_a G^0_{AB,P,T} = \Delta_f H^0_{AB,P,T} - T \cdot S^0_{AB,P,T}$$

$$= \Delta_f H^0_{AB,Pr,Tr} - T \cdot S^0_{AB,Pr,Tr} + \int_{Tr}^{T} C^0_{p,AB} dT - T \cdot \int_{Tr}^{T} \frac{C^0_{p,AB}}{T} dT + \int_{Pr}^{P} V^0_{AB} dP \quad (1)$$

where T_r: temperature at the reference state (298.15 K); P_r: pressure at the reference state (0.1 MPa); $\Delta_f H^0_{AB,P,T}$: enthalpy of formation of the phase AB at temperature T and pressure P; $S^0_{AB,P,T}$: the third law entropy of the AB phase; $C^0_{p,AB}$: heat capacity of the AB phase; V^0_{AB}: molar volume of the AB phase, independently of temperature.

This definition follows the Benson–Helgeson convention (Benson, 1968; Helgeson et al., 1978) where $\Delta_a G^0_{AB,P,T}$ equals $\Delta_f G^0_{AB,P,T}$ only at 25°C. The heat capacity function is related to the dependence of entropy and formation enthalpy with temperature through:

$$\Delta_a H^0_{AB,P,T} = \Delta_f H^0_{AB,Tr} + \int_{Tr}^{T} C^0_{p,AB} dT \text{ and } S^0_{AB,P,T} = S^0_{AB,Tr} + \int_{Tr}^{T} \frac{C^0_{p,AB}}{T} dT \quad (1)$$

The third law entropy term, at T_r, includes the heat capacity function, and a residual contribution:

$$S^0_{AB,Pr,Tr} = \int_0^{Tr} \frac{C^0_{p,AB}}{T} dT + S^{mag}_{AB} + S^{conf}_{AB} \text{ where } \int_0^{Tr} \frac{C^0_{p,AB}}{T} dT = S^{lat}_{AB,Pr,Tr} \quad (3)$$

with $S^{lat}_{AB,Pr,Tr}$ standing for the lattice entropy. The two first terms in Equation (3) can be measured by low temperature calorimetry (PPMS or adiabatic, Gailhanou et al. (2012)) and S^{mag}_{AB} represents the magnetic entropy (Holland, 1989). For the configuration entropy term S^{conf}_{AB}, Ulbrich and Waldbaum (1976) proposed a calculation method for assessing the maximum value of both the magnetic and the configurational entropy terms. For the S^{conf}_{AB} term, the method is based on a site mixing approach and for the magnetic contribution, on the maximum number of spin configurations according to:

$$S^{mag}_{AB} = R \sum_i x_i^{AB} \ln(2S_i + 1) \quad (4)$$

where R is the gas constant, x_i^{AB} the mole fraction of element i in solid AB, and S_i its spin number. This expression is valid for the metals of the first transition series for which the valence electrons are in the outermost shells.

The illite/smectite case needs to define solid solution properties. Considering a second solid phase CB, its Gibbs free energy $\Delta_f G^0_{SS,P,T}$ results from the combination of both end-members' Gibbs free energy, $\Delta_f G^0_{AB,P,T}$ and $\Delta_f G^0_{CB,P,T}$ by :

$$\Delta_f G^0_{SS,P,T} = x \cdot \Delta_f G^0_{AB,P,T} + (1-x)\Delta_f G^0_{CB,P,T} + \Delta G^{mix}_{SS,P,T} \quad (5)$$

where x and $\Delta G^{mix}_{SS,P,T}$ correspond respectively to the fraction of AB end-member and the Gibbs energy of mixing. The latter can be decomposed into enthalpy $\Delta H^{mix}_{SS,P,T}$ and entropy $\Delta S^{mix}_{SS,P,T}$ of mixing terms:

$$\Delta G^{mix}_{SS,P,T} = \Delta H^{mix}_{SS,P,T} - T \cdot \Delta S^{mix}_{SS,P,T} \quad (6)$$

The entropy of mixing can be estimated, to a first approximation, considering an ideal mixing between end-members, resulting in:

$$\Delta S^{mix}_{SS,P,T} = -R \cdot [x\ln(x) + (1-x)\ln(1-x)] \quad (7)$$

As for the equilibrium of AB in an aqueous solution, we consider the dissolved species A^+ and B^- and the chemical reaction:

$$AB \overset{\Delta_r \Xi^0_{AB,P,T}}{\longleftrightarrow} A^+ + B^- \quad (8)$$

Any reaction property $\Delta_r \Xi^0_{AB,P,T}$ can be obtained from the corresponding formation property $\Delta_f \Xi^0_{AB,P,T}$, according to the relation:

$$\Delta_r \Xi^0_{AB,P,T} = \Delta_f \Xi^0_{A+,P,T} + \Delta_f \Xi^0_{B-,P,T} - \Delta_f \Xi^0_{AB,P,T} \quad (9)$$

where Ξ stands for G, H or S, or any other property. Finally, the Gibbs free energy of reaction (3) is related to the equilibrium constant of the reaction, $K_{AB,P,T}$, by:

$$\Delta_r G^0_{AB,P,T} = -R \cdot T \cdot \mathrm{Log}K_{AB,P,T} \cdot \ln(10) \quad (10)$$

$$\Delta_r G^0_{AB,P,T} = -R \cdot T \cdot \log_{10} K_{AB,P,T} \cdot \ln(10)$$

Clay minerals may undergo hydration reactions (smectites and vermiculites). In more detail (Gailhanou et al., 2017), a hydration reaction may be expressed by:

$$\text{dehydrated clay} + n \cdot H_2O \leftrightarrow \text{hydrated clay}, nH_2O \quad (11)$$

We can consider the property of hydration $\Delta\Xi^0_{hyd,Tr}$ (per H_2O mole) for a given clay mineral having n bounded molecules per half-cell. It is related to the total formation property $\Delta\Xi^0_{f,Tr}$ of the mineral through the following relation:

$$\Delta_f \Xi^0_{Pr,Tr}(\text{hydrated clay}) = \Delta_f \Xi^0_{Pr,Tr}(\text{anhydrous clay}) + n_{H2O} \cdot \Delta_f \Xi^0_{Pr,Tr}(H_2O) + n_{H2O} \cdot \Delta_{hyd} \Xi^0_{Pr,Tr} \quad (12)$$

where $\Delta_f \Xi^0_{Pr,Tr}(\text{hydrated clay})$, $\Delta_f \Xi^0_{Pr,Tr}(\text{dehydrated clay})$ and $\Delta_f \Xi^0_{Pr,Tr}(H_2O)$ stand for the formation property for the hydrated mineral, the dehydrated mineral and the bulk water, respectively.

Regarding clay minerals, in order to estimate the whole set of thermodynamic parameters, including the hydration properties, it is necessary to combine models able to predict

anhydrous phase properties and models able to calculate the hydration properties. Such a methodology had been previously followed by Vidal et al. (2009) and Dubacq et al. (2010), who combined their own hydration model with Chermak and Rimstidt's work (1989), for the anhydrous part. Similarly, in this study the estimatation of thermodynamic properties for hydrated clay minerals is achieved by merging the model of Blanc et al. (2015) for the anhydrous part and the model developed by Gailhanou et al. (2017) and Vieillard et al. (2019) for hydration. The whole process is illustrated in Figure 1.

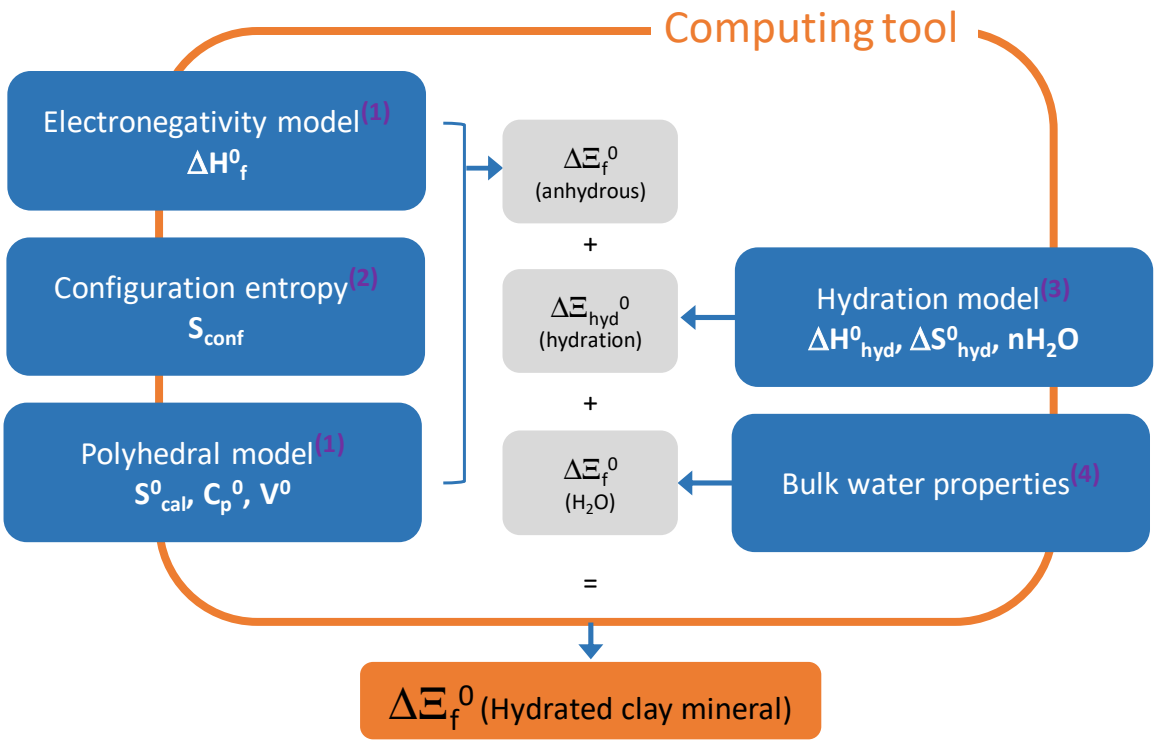

(1) Vieillard et al. (1994a and b), Blanc et al. (2015) ; (2) Ulrich and Waldbaum (1976) ; (3) Gailhanou et al. (2017), Vieillard et al. (2019) ; (4) Cox et al. (1989)

Figure 1 – General scheme indicating the relations between estimation models to provide thermodynamic properties for hydrated clay minerals

4. Generic estimation tool: ClayTherm

The calculation of cation sharing in crystallographic sites has been automated in a computing tool, giving the opportunity to improve the Blanc et al. (2015) model in terms of consistency and to provide additional verification cases. These aspects are described below.

4.1. AUTOMATION OF CATION SHARING IN CRYSTALLOGRAPHIC SITES

Minerals with d-spacings of 7, 10 and 14 Å contain M1 and M2 octahedral sites (1 M1 and 2 M2 per $O_{10}(OH)_2$). In Blanc et al. (2015), the sharing of cations was calculated based on a random distribution, with 2/3 of the cations entering M2 sites and 1/3 M1 sites. Such an assumption is valid for trioctahedral minerals, for which all sites are filled with mostly divalent species. For dioctahedral minerals with an octahedral composition dominated by trivalent species and composition close to 2 cations per $O_{10}(OH)_2$, automatically applying this sharing method implies creating vacancies in M2 sites, which does not correspond to current crystallographic observations (Brown, 1982). In this regard, the calculation should include a rule so as for dioctahedral minerals to fill in the M2 sites up until 2 cations per $O_{10}(OH)_2$. Additional cations, for a dioctahedral mineral with more than 2 octahedral cations, are thereafter entering the M1 site. The limit to this infilling process was pointed out by Yamada et al. (1999). They investigated the dioctahedral-trioctahedral 2:1 smectite join, from experiments and reviewing previous literature data. They concluded that there was a large miscibility gap between 2.33 and 2.66 cations per $O_{10}(OH)_2$. Following this, starting from 2 up to 2.33 cations per $O_{10}(OH)_2$, M1 and M2 sites are filled proportionally to the relative amounts. From 2.33 to 2.66 cations, no phase should be stable and between 2.66 and 3 cations, the mineral is reported to be trioctahedral, without cation preferences between M1 and M2 sites (Yamada et al., 1999). Eastonite $K(Mg_2Al)(Si_2Al_2)O_{10}(OH)_2$, an end-member of the biotite solid solution, represents a specific case. Circone and Navrotsky (1992) reported, based on infrared and Raman spectra of Mg-Al-biotite, that Al orders onto the M1 site. Al ordering in M1 is considered in the model developed by Blanc et al. (2015). This type of ordering is implemented as a specific option, which also applies to siderophyllite. The option also includes Si, Al ordering between T1 and T2 tetrahedral sites. Globally, the thermodynamic properties of biotite solid solution end-members phlogopite, annite, eastonite and siderophyllite can be correctly estimated. But for intermediate compositions, neither miscibility gaps nor the cation order/disorder relations (Dachs and Benisek, 2019) have been implemented, so far. This limits the use of the tool for minerals belonging to the Biotite group.

Regarding (Si, Al) sharing in T1 and T2 tetrahedral phyllosilicate sites, Vinograd (1995) compiled the measurements performed on many silicates (including phyllosilicates). He concluded that (Si, Al) ordering was only partial among the tetrahedral sites, according to the Homogeneous Distribution of Charge (HDC) hypothesis and depending on the Al/(Al+Si) ratio. Globally, for an Al/(Al+Si) ratio from 0 to 0.1, few analyses are available in the literature and the distribution model impact on entropy is limited. For an Al/(Al+Si) ratio above 0.35, the Al-ordering between T1 and T2, corresponding to the Al-avoidance rule, would apply. At an Al/(Al + Si) ratio ranging from 0.2 to 0.35, a distribution based on the HDC hypothesis would provide better consistency with Vinograd (1995). The three distributions, i.e. disordered, ordered and HDC (Vinograd, 1995), are implemented in the present calculation tool.

For 10Å minerals, the entropy contribution of the interlayer configuration sites is calculated according to the Ulbrich and Waldbaum (1976) method, including mixing with vacancies. For the 14Å mineral brucite layer, sharing is calculated according to the Holland and Powell

(1998) method. The latter consists in distributing Al preferentially in the M4 site, then randomly sharing the remaining octahedral cations in the M1, M2 and M3 sites.

For most of the 7Å minerals, the chemical composition does not greatly differ from that of the end-members. In this case, there is a general tendency to neglect the configurational entropy contribution (Bertoldi et al., 2005; Blanc et al., 2014), which we adopted here. Similarly and following Hemingway et al. (1984), the configurational contribution was not considered in this work for 14Å minerals. In contrast and following Holland (1989), for 10Å minerals Blanc et al. (2015) considered both the configuration and the additional terms of the magnetic entropy, whose calculation is also included in the overall calculation, consistently to Equation (3).

4.2. EXTENDING THE COMPOSITION LIMITS OF PREVIOUS MODELS

In the work presented by Blanc et al. (2015), the chemical elements which can be considered for both entropy and enthalpy estimates do not exactly match. The development reported in this article provides an opportunity to improve consistency, from this point of view. For S^{lat}, C_p^0 and V^0 estimates, the basic unit properties have been assessed according to the method described by Blanc et al. (2015), for interlayer NH_4^+, octahedral Cd^{2+} and tetrahedral Fe^{3+} (see Table 1). It allows the set of basic units to be completed, consistently with the elements considered for enthalpy estimates by Blanc et al. (2015).

Table 1 - Thermodynamic properties for additional polyhedral units (after Blanc et al. 2015)

	S^{lat}	C_p^0	V^0
	$J.mol^{-1}.K^{-1}$	$J.mol^{-1}.K^{-1}$	$cm^3.mol^{-1}$
$^{[int]}(NH_4)_2O$	364.50	247.63	38.16
$^{[6]}CdO$	52.23	41.95	13.11
$^{[4]}Fe_2O_3$	66.62	101.33	27.29

Bracketed numbers: correspond to the coordination of the cation in the phyllosilicate structure

4.3. IMPLEMENTATION OF THE CALCULATION IN CLAYTHERM

The tool ClayTherm was developed in Visual Basic©, under the Excel© interface. It estimates the formation and reaction properties for 7, 10 and 14Å anhydrous minerals and 10Å hydrated phases. To facilitate the implementation in most geochemical databases, the temperature dependence of the equilibrium constant, $\log_{10}K(T)$, is calculated for 8 temperatures (0, 25, 60, 100, 150, 200, 250, 300°C), using the Cp constant approximation, and the parameters A, C and D for the function $\log_{10}K(T) = A + C/T + D \cdot log_{10}(T)$ are provided. Thermodynamic properties of ions are issued from the Thermochimie database (Giffaut et al., 2014) and are consistent with the Thermoddem database (Blanc et al., 2012). The sharing of the cations throughout the different crystallographic sites is calculated automatically, according to the rules previously reported.

4.4. TESTING OF CLAYTHERM

A first testing phase was conducted by running the tool for phases considered by Blanc et al. (2015) and Vieillard et al. (2019). A second testing phase was conducted by comparing the solubilities obtained by Gaboreau et al. (2020) with predicted values. The work on illite/smectite provides an opportunity for additional testing (see below).

4.4.1. Comparison with Blanc et al. (2015) and Vieillard et al. (2019) datasets

The minerals used to parameterize the model developed by Blanc et al. (2015) (Table 12, Blanc et al. 2015) were first tested, to check the consistency of the tool developed here:

- 14Å minerals: (Si, Al) ordered, no deviation
- 10Å minerals: HDC Vinograd (1995) model except for eastonite and siderophyllite (Si, Al), the ordered octahedral layer and for paragonite which is (Si, Al) ordered. A typographical error was detected in Blanc et al. (2015) where paragonite S^{lat} should equal 305.20 instead of 305.31 $J.mol^{-1}.K^{-1}$
- 7Å minerals: (Si, Al) ordered, no deviation.

For the 10Å anhydrous and hydrated end-members calculated in Blanc et al. (2015) (Table 14) and Vieillard et al. (2019) (Table 8), the results are identical using the HDC ordering model. Two differences arises for the 7Å minerals Berthierine(FeII) and Cronstedtite (Blanc et al. 2015, Table 14). Berthierine(FeII) $\Delta_f H^0$ displays a typographical error in Blanc et al. (2015) with -3770.46 instead of -3775.46 $kJ.mol^{-1}$, the correct value provided by ClayTherm. For Cronstedtite, the calculation from Blanc et al. (2015) was limited by using a $^{[4]}Fe_2O_3$ component assessed using Goethite properties. Now this component is fully integrated in ClayTherm which modifies the thermodynamic properties:

- Blanc et al. (2015): $\Delta_f H^0$ =-2914.55 $kJ.mol^{-1}$; S^{lat} = 256.60 $J.mol^{-1}.K^{-1}$; C_p^0 = 257.02 $J.mol^{-1}.K^{-1}$; V^0 = 76.80 $cm^3.mol^{-1}$
- This work: $\Delta_f H^0$ = -2916.68 $kJ.mol^{-1}$; S^{lat} = 289.91 $J.mol^{-1}.K^{-1}$; C_p^0 = 307.69 $J.mol^{-1}.K^{-1}$; V^0 = 90.44 $cm^3.mol^{-1}$

On the whole, the comparison with the results of Blanc et al. (2015) and Vieillard et al. (2019) confirms that ClayTherm results are correct for most clay minerals. It allows typographical errors to be corrected and the predicted properties of cronstedtite to be improved, with respect to Blanc et al. (2015).

4.4.2. Comparison with solubility datasets

Vieillard et al. (2019) proposed a first selection of solubility data from the literature and comparison with $\log_{10}K$ (298.15 K) estimates gives an average of ± 2.5 $\log_{10}$ units. The selection was recently refined by Gaboreau et al. (2020) who also reported a new set of experimentally measured solubilities for clay minerals: kaolinite, smectite, illite, vermiculite and chlorite. For the latter, equilibrium was clearly not reached, even after 2 years of equilibration at 40°C. Additionally, they selected a set of solubility experiments, from previous literature. Both sets were used in the present study to assess the estimates obtained using ClayTherm.

Results for the testing of the set of solubility data obtained by Gaboreau et al. (2020) are reported in Table 2. Globally, estimates correspond to solubilities with a rather low standard deviation between both values (± 0.41 $\log_{10}$ units). Overall, the difference with estimates is larger when considering calorimetric data, especially due to the contribution of vermiculite (3.85 $\log_{10}$ units). The vermiculite Santa Ollala sample purified by Gailhanou et al. (2013) for the calorimetric measurements still contains an amount of impurities, like organic carbon, of which 0.42 wt. % still remains, even after H_2O_2 treatment. Such impurity, not considered in the thermodynamic cycle used to derive formation enthalpy, could affect the correctness of the extracted value.

Standard deviations can be calculated from Table 2, for differences reported in columns 9 and 10. Without considering chlorite solubility, the standard deviation is ± 1.3 or ± 0.4 log_{10} units, depending whether or not calorimetry for vermiculite is considered. The average of both standard deviations, i.e. ± 0.9 log_{10} units, produces a rather high uncertainty for $log_{10}K$ (298.15 K) estimates (± 1.7 log_{10} units). This is still the most reasonable statement that can be made concerning uncertainties for $log_{10}K$ (298.15 K) estimates in this work.

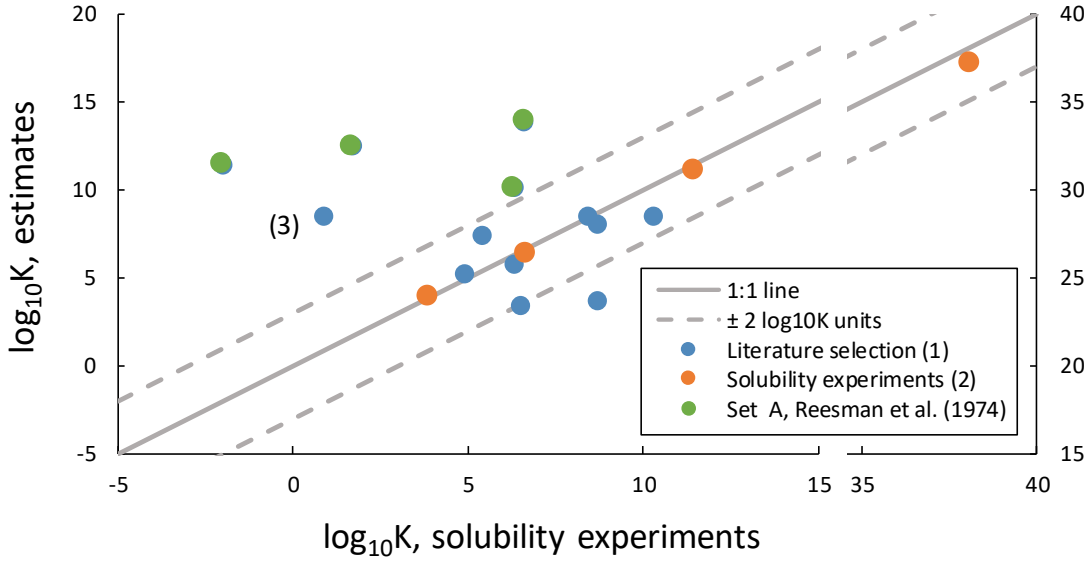

Figure 2 – Comparison between $log_{10}K$ (298.15 K) ClayTherm estimates and results from previous literature studies: (1) kaolinite, smectite, illite and vermiculite from Gaboreau et al. (2020); (2) Illites and smectites from Gaboreau et al. (2020) literature selection.

Table 2 - Comparison between Gaboreau et al. (2020) experiment $log_{10}K$ (298.15 K) and ClayTherm estimates

		Temp. (°C)	Solution exp. $log_{10}K$[5]	(±)	Calorimetry $log_{10}K$	(±)	Estimate $log_{10}K$	Δ (Sol-Est)[a]	Δ (Cal-Est)[b]
Kaolinite KGa-2[1]	$Si_2Al_{1.98}Fe_{0.02}O_5(OH)_4$	40	6.61	0.70	6.46	0.60	6.40	0.21	0.06
Illite IMt-2[2]	$K_{0.762}Na_{0.044}(Si_{3.387}Al_{0.613})(Al_{1.427}Mg_{0.241}Fe^{3+}_{0.292}Fe^{2+}_{0.084})O_{10}(OH)_2$	25	11.42	0.70	11.52	1.60	11.15	0.27	0.37
Smectite MX80[2]	$Na_{0.409}K_{0.024}Ca_{0.009}(Si_{3.738}Al_{0.262})(Al_{1.598}Mg_{0.214}Fe^{3+}_{0.173}Fe^{2+}_{0.035})O_{10}(OH)_2{\cdot}5.189H_2O$	40	3.83	1.70	3.33	1.70	3.88	-0.05	-0.55
Vermiculite SO[3]	$Ca_{0.445}(Si_{2.778}Al_{1.222})(Al_{0.216}Mg_{2.475}Fe^{3+}_{0.226}Fe^{2+}_{0.028})O_{10}(OH)_2$	40	38.07	0.70	41.01	1.40	37.16	0.91	3.85
Chlorite CCa-2[4]	$(Si_{2.633}Al_{1.367})(Al_{1.116}Mg_{2.964}Fe^{3+}_{0.215}Fe^{2+}_{1.712}Ca_{0.011})O_{10}(OH)_8$	40	46.49	0.90	56.01	1.30	55.93	-9.44	0.08

References: (1) Blanc et al. (2015) ; (2) Gailhanou et al. (2012) ; (3) Gailhanou et al. (2013); (4) Blanc et al. (2014); (5) Gaboreau et al. (2020)

[a]: $log_{10}K$ (298.15 K) differences between solubility and estimates

[b]: $log_{10}K$ (298.15 K) differences between calorimetry and estimates

As illustrated in Figure 2, ClayTherm predictions are in very good agreement with the solubilities measured by Gaboreau et al. (2020). The relation is still correct with the equilibrium constants extracted from literature by Gaboreau et al. (2020), provided the set of data from Reesman (1974) is discarded (set A in Figure 2). The reason for discarding this dataset could lie in the unusually high liquid/solid ratio L/S = 200 used by the authors, almost ten times higher than the ratio L/S=24 used by Misra and Upchurch (1976) and Gaboreau et al. (2020). A high L/S ratio could delay the duration required to reach equilibrium and to overestimate the stability of the mineral. The last point strongly departs from the general tendency, point (3) in Figure 2, which corresponds to the equilibrium constant extracted by Huang and Keller (1973) for the Fithian illite. It is interesting to note that the analysis provided by the authors strongly differs from that provided by Reesman (1974). Furthermore, Huang and Keller (1973) do not explain the source of data for the mineral analyses, which could raise questions especially concerning the constant extracted for the Fithian Illite. Except for Reesman (1974) data and Huang and Keller (1973) Fithian illite data, all other constants are globally located within a ± 2.0 $\log_{10}K$ (298.15 K) interval. This interval is close to the ±1.7 $\log_{10}K$ (298.15 K) previously deduced for the estimates, meaning that the estimated values are consistent with the solubility data selected from previous literature and displayed in Figure 2.

5. Calculation tool to derive illite/smectite compositions: ISTherm

A specific application and dedicated development are provided for the stability of illite/smectite interstatified minerals (I/S). Geloni et al. (2017) previously proposed a first application, based on Blanc et al. (2015), to estimate the thermodynamic properties of I/S minerals. This work introduces an evolution of the concept, integrating composition calculations and non-ideal mixing energies. Indeed, the goal of this second tool (ISTherm) is, from a given I/S composition, to derive the detailed composition of the smectite and illite end-members and intermediate compositions, according to the composition trend to which the I/S of interest belongs. ISTherm is a macro-enabled Microsoft Excel© file available upon request.

5.1. ILLITE/SMECTITE SOLID SOLUTION MODEL

Gailhanou et al. (2019) reported the measurements of thermodynamic properties for an I/S mineral of given composition (ISCz-1, from the Source Clay repository). This measurement is used here to support the development and the verification of an I/S solid solution model and its implementation into a predicting tool.

5.1.1. End-members composition calculation

According to Meunier and Velde (1989), the smectite-to-illite transformation reaction follows pre-determined composition trends. In particular, as shown in Figure 3, the I/S composition field has a triangular shape defined by a single illite end-member and two smectite end-members, which differ in the composition of the octahedral layer.

Meunier and Velde (1989) showed that smectite composition evolves, with increasing temperature during diagenesis, from a compositional area lying along the Montmorillonite line (mnt0.33/mnt0.66, Figure 3), towards the Illite 0.85 end-member. This evolutionary path is recognizable as a linear trend within the trilinear space defined by the following end-members: (i) 4Si (the number of Si per $O_{10}(OH)_2$, divided by 4), (ii) R^{2+} (the number of octahedral divalent cations) and (iii) M^{+} (the total charge deficit). Despite this evidence, it is important to note that the three aforementioned parameters (4Si, R^{2+} and M^{+}) cannot fully describe, in terms of interlayer cations (K^{+}, Na^{+}, Mg^{2+} or Ca^{2+}), octahedral cations (Mg^{2+}, Fe^{2+}, Fe^{3+}, Al^{3+}) or tetrahedral cations (Si^{4+} and Al^{3+}), the complex composition of I/S minerals.

The approach of Meunier and Velde (1989) was revisited by Meunier et al. (2004) for the presence of vermiculite layers in the stacking sequence of some I/S minerals. Such modifications can explain the increase in the tetrahedral charge for the montmorillonite component. These considerations are beyond the scope of the present work but they could be the focus of further developments for the model presented here.

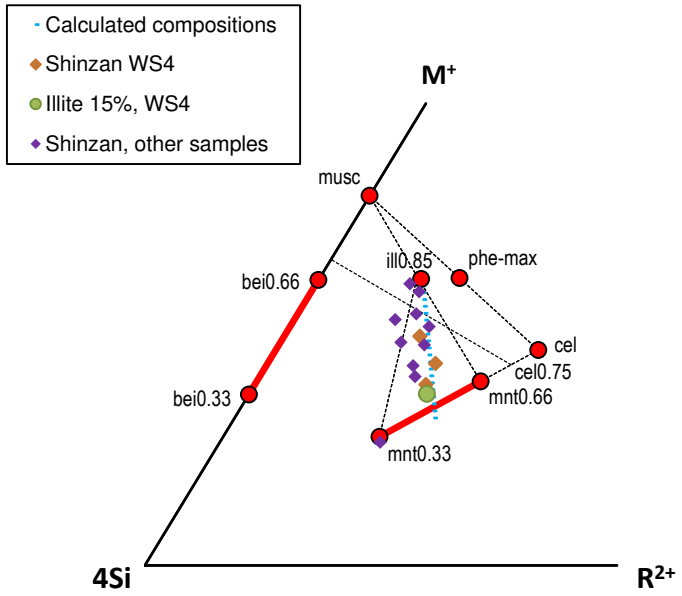

Figure 3 - *4Si-R^{2+}-M^{+} projection displaying smectite-to-illite evolution trends, after Meunier and Velde, 1989.*
Abbreviations: musc: muscovite; bei: beidellite; cel: celadonite; phe: phengite; mnt montmorillonite; ill: illite

The calculation tool ISTherm implements the approach developed by Meunier and Velde (1989) to calculate intermediate compositions along the trend joining the composition of the sample and the illite end member, up to the montmorillonite composition line (see Figure 3).

The tool first calculates the composition of the illite and smectite end-members, based on their coordinates in the 4Si-R^{2+}-M^{+} projection. Then, 20 intermediate compositions are determined, by increasing the illite content from the smectite end-member. The results of the calculation are illustrated in Figure 3 for the Shinzan I/S series (Gailhanou, 2005). The following points should be emphasized:

- The calculation implies that the number of octahedral cations is equal to that of the mineral composition considered, the same value for smectite and illite end-members and intermediate compositions;
- End-member coordinates in the 4Si-R^{2+}-M^{+} projection determine the tetrahedral, octahedral and total layer charge. The tool calculates the linear variations of the charge between end-members and it provides the charge values for each of the intermediate compositions;
- Cations are distributed randomly among the different crystallographic sites;
- For sake of simplicity, the tool provides the possibility to replace Ti by Al and Mn by Mg.

5.1.2. Thermodynamic properties of the solid solution

The thermodynamic properties of illite/smectite interstratified minerals have been investigated following three distinct approaches:

- by applying the global model implemented in ClayTherm to intermediate compositions corresponding to average values between the illite and smectite end-member;

- by considering a mechanical mixture of illite and smectite, i.e. by removing the energy of mixing term from Equation (5);
- by considering a mechanical mixture that accounts for the energies of mixing (ideal + non-ideal).

The results of the different approaches are discussed below, after an introductory section on the calculation methods used to estimate the mixing properties.

The enthalpy of mixing ΔH^{mix} can be directly obtained from the calorimetric measurements performed on the I/S series from the Shinzan area by Gailhanou (2005) and Gailhanou et al. (2019). These measurements are reported in Figure 4. A semi-empirical function was developed to address ΔH^{mix} variations with respect to smectite fraction X_{sm} in illite/smectite:

$$\Delta H^{mix} = x_{sm} \cdot (36.01 \cdot x_{sm} \cdot R^{2+} - 19.03) \quad (13)$$

This function not only depends on the smectite fraction (as expected for an illite/smectite interaction term) but it also includes an octahedral composition dependence, to account for the variability observed for the Shinzan samples (Gailhanou, 2005). For comparison, the results provided using the solid solution model developed by Blanc et al. (1997) are also displayed (Figure 4). This model includes short range ordering and was parameterized considering diagenetic illite/smectite series. The results are similar to the measurements, at least for R1 ordered I/S samples (illite > 55 to 60 %). For the smectite-rich minerals, Blanc et al. (1997) considered that the disordered I/S stacking sequence implied $\Delta H^{mix} = 0\ \mathrm{J.mol^{-1}}$. This statement is wrong, given the experiment results displayed in Figure 4. In this work, the function from Equation (13) is complemented with an ideal entropy of mixing term, as in Equation (7), to calculate the Gibbs energy of mixing used in Figure 5. This choice allows quite a simple hypothesis to be tested, knowing that more complex expressions have been developed, especially to include the influence of ordering in the expression of the entropy of mixing (Blanc et al., 1997).

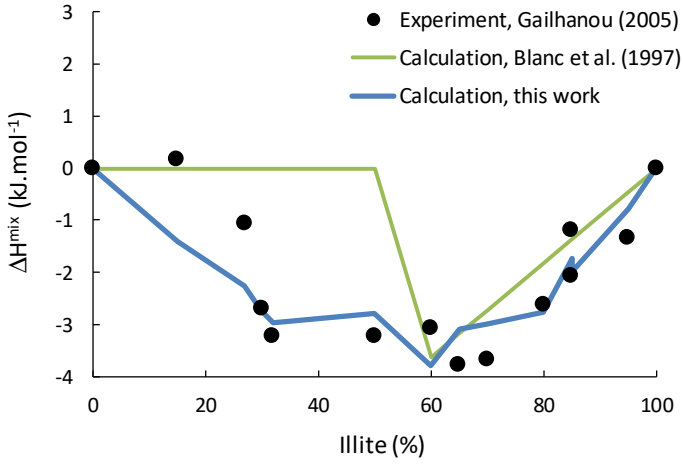

Figure 4 – Enthalpies of mixing determined for Shinzan series of samples from Gailhanou (2005) measurements

Figure 5 illustrates the differences, in terms of Gibbs energy (ΔG^{mix}), between the three different methods used to estimate I/S thermodynamic properties, i.e. the global model (ClayTherm), the mechanical mixture and the non-ideal mixture. The curves displayed in Figure 5 correspond to the Gibbs energy differences between the global model and the

mechanical mixture or the non-ideal mixture models, respectively. I/S compositions correspond to samples from the Shinzan series studied by Gailhanou (2005) and Gailhanou et al. (2019). Since the differences are globally negative, it implies that the mixture of illite and smectite layers stabilizes I/S of intermediate composition. This effect is enhanced when considering the mixing terms in the solid solution model, consistently with the negative enthalpies of mixing measured by Gailhanou (2005) and Gailhanou et al. (2019) and displayed in Figure 4.

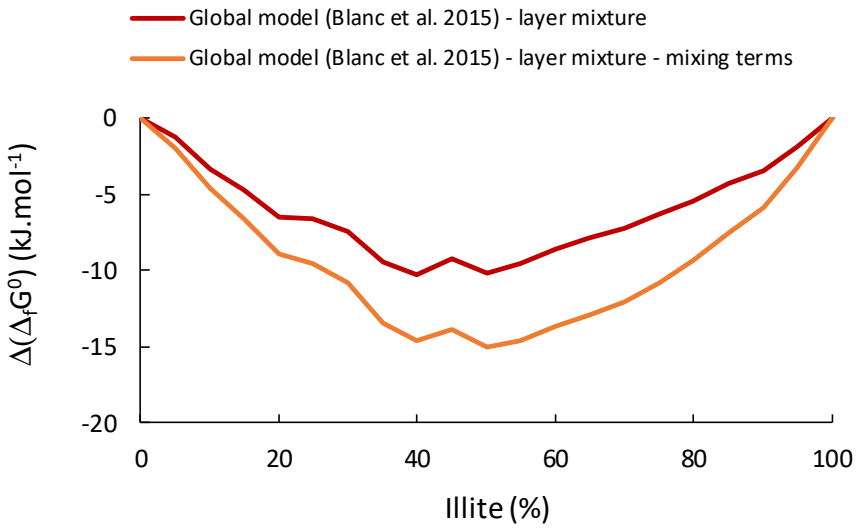

Figure 5 – *Estimates of illite/smectite Gibbs free energy of mixing for Shinzan series (composition of samples after Gailhanou et al., 2019).*

Similar calculations were performed by Gailhanou et al. (2019) for the ISCz-1 sample. The $\Delta_f G^0$ estimated by the authors is also closest to the experiment values (Δ < 0.01 %) when non-ideal mixture of illite and smectite layers is considered. In addition, ISCz-1 disappears from the stable phases when $\Delta_f G^0$ is estimated using the global model. It re-appears among the stable phases when considering a non-ideal mixture of illite and smectite layers for the $\Delta_f G^0$ estimate calculation. This comparison enforces the use of the non-ideal model for I/S estimates.

5.2. APPLICATION TO THE SHINZAN SERIES CASE

A series of fourteen illite-smectite mixed-layer samples taken from the Shinzan area, northeast Japan, was also used for this study. This series, well described in the literature (Inoue et al., 1987; Inoue and Utada, 1983), is noticeable as it consists in a complete mixed-layer series with chemical compositions varying from montmorillonite to illite end-members. The series results from the hydrothermal alteration of dioctahedral micas/smectites. The continuous conversion of smectite into illite has been described by Inoue et al. (1987). The main transformation mechanism suggested by the authors was based on the dissolution of smectite and the crystallization of illite. A solid-state transformation mechanism was also shown from HRTEM observations (Amouric and Olives, 1991; Olives et al., 2000).

5.2.1. Stability diagrams for the WS4 Shinzan series

Considering the full composition of a sample from the WS4 borehole (sample B in Gailhanou 2005), the calculation tool is used in order to calculate the composition and thermodynamic properties of a series of 10 I/S with an amount of illite ranging from 0% (pure smectite) to 100% (pure illite). This series was selected because it displays a central location in the illite-mnt0.33-mnt0.66 triangle (see Figure 3). These compositions are reported in Figure 2, together with the fourteen samples from the Shinzan area analysed by Gailhanou (2005). The thermodynamic properties and detailed composition of the samples are presented in Annex 1 (supplementary data). The stability fields of each I/S composition are represented in Figure 6A to D, at 25 and 150°C, for anhydrous and hydrated I/S phases. Figures 6 also present the solution compositions collected by Aagaard and Helgeson (1983) and used by Aagaard and Helgeson (1983) and Garrels (1984) to illustrate the illite/smectite stability fields. I/S phases are supplemented to the original Aagaard and Helgeson (1983) legend, in agreement with the discussion presented by the authors. The agreement between the mineralogical assemblage in contact with solutions and the stability fileds is globally correct for Figure 6.D, drawn at 25°C for hydrated I/S phases. This corresponds to the subsurface condition of water sampling, in the studies selected by Aagaard and Helgeson (1983). At 25°C (Figure 6.B), the stability field of anhydrous I/S phases is globally shifted toward the high silica activities, which is not in agreement with the location of the solutions in contact with mineral assemblages including montmorillonite. At higher temperatures (Figures 6.A and 6.C), differences between anhydrous and hydrated I/S are more limited, consistently with the decrease of I/S in the clay water when the smectite fraction decreases. From Figures 6.A and 6.C, a temperature increase induces the displacement of the stability fields toward the high silica activities, which stabilizes illite-rich I/S compositions, consistently with the I/S composition evolution during diagenesis (Velde and Vasseur, 1992). This effect would even be reinforced by the transition from Opal-A to Opal-CT to quartz, occurring in early diagenetic sequences (Compton, 1991), over long periods of time and a temperature rise, which would naturally decrease the silica activity.

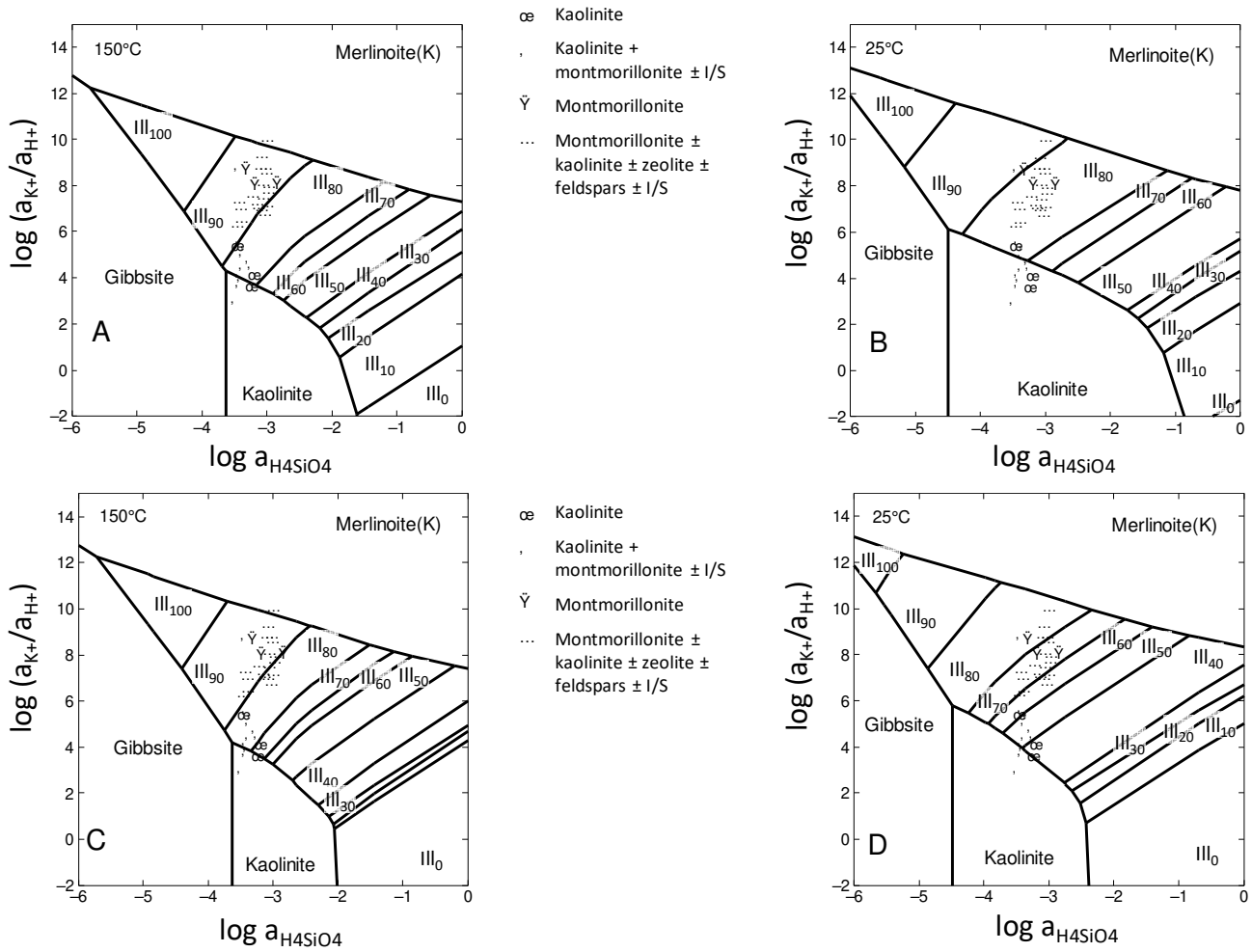

Figure 6 – *I/S stability fields calculated for the WS4 Shinzan series, anhydrous phases: A) at 150°C, B) at 25°C; hydrated phases: C) at 150°C, D) at 25°C*

Concentrations of elements other than Si, K or Al are established by stating the equilibrium with the following minerals: anorthite (Ca), albite (Na), lizardite (Mg), magnetite and ferrihydrite (Fe and dissolved O_2)

5.2.2. Reactive transport modelling: case of the WS4 Shinzan series

This section presents a case of preliminary reactive transport calculation for the WS4 Shinzan geothermal borehole (Shinzan area, Akita Prefecture, Northeast Japan). The calculation aims to reproduce the progressive illitization of a smectite-rich formation, altered by a geothermal hot fluid. These calculations imply different hypotheses for the geological formation and the hydrothermal fluids, which rely on previous literature observations and measurements. Lacking compositions or parameters were addressed by analogy with similar contexts. This exercise highlights the potential and some weaknesses for illitization geochemical modelling, based on the developments presented in this work.

The Shinzan area, covered by quaternary sediments, presents two pyroclastic Miocene formations, which have been subjected to hydrothermal alteration. A vertical cross-section representing the Shinzan geothermal field with the main boreholes is given in Figure 7.

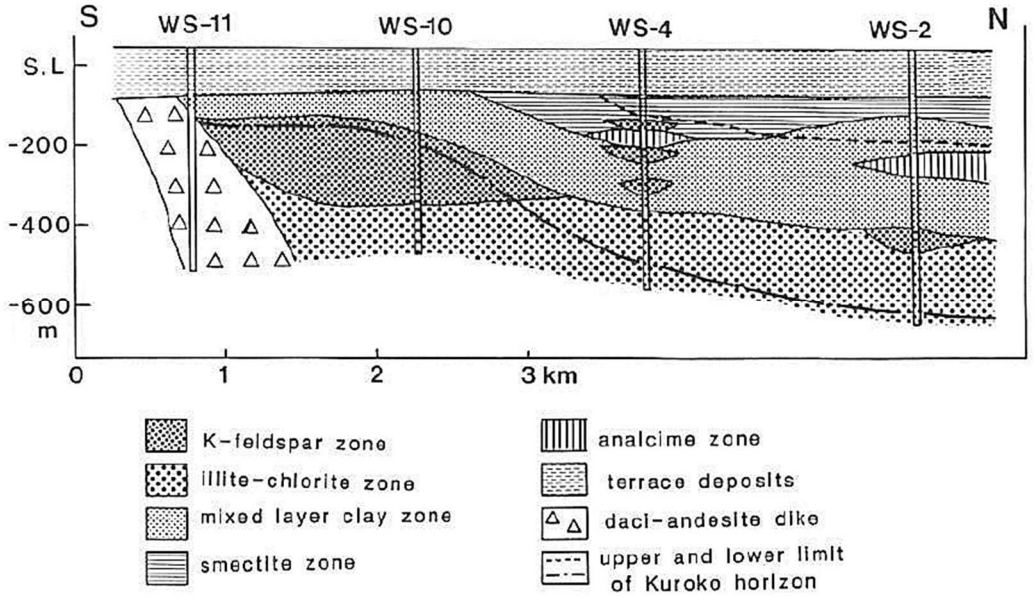

Figure 7 – *Distribution of the mineral zones in the Shinzan field (after Inoue et al. (1992))*

Initial materials and fluids

The composition of the geothermal fluid proposed by Inoue and Utada (1983) is given in Table 3. The fluid chemistry considered in calculations was established by processing a first geochemical calculation, assuming a temperature of 220°C, based on the work published by Inoue et al. (1992) (Figure 6 in Inoue et al., 1992). In this calculation, thermodynamic equilibrium is assumed between the solution and a mineralogical assemblage made of quartz, pure illite and gibbsite, in order to constrain Si, Mg and Al concentrations, i.e. concentrations not or roughly estimated by Inoue and Udata (1983). A CO_2 partial pressure of 0.1 bar was considered, typical of underground environments (Coudrain-Ribstein et al., 1998).

The compositions and thermodynamic properties of an I/S series was calculated using ISTherm, based on sample B from the WS4 series (Gailhanou, 2005), as reported in the previous section. For the present calculation, only anhydrous minerals were considered, for sake of simplicity and because the difference, in terms of stability, between hydrated and

anhydrous minerals is lower at high temperature (Figures 6.A and 6.C). A calculation case using hydrated compositions showed no significant differences with the results reported here. The composition of the I/S minerals is represented in Figure 3, their thermodynamic properties are provided in Annex 1 and their stability fields are reported in Figure 6.

The works published by Inoue and Utada (1983) and Inoue et al. (1987, 1992) on the Shinzan claystone focus on the smectite-to-illite conversion. Limited information is provided concerning accessory minerals. For the smectite-rich formation, a simple assumption is considered with pure smectite as the starting material, with traces of gibbsite and quartz, to help control dissolved silica and alumina in the first steps of the reaction. A porosity of 20 % was also arbitrarily considered.

Table 3 - *Composition of the geothermal fluid and associated mineralogy (in mol.L^{-1}).*

	Hydrothermal fluid		Initial formation
	Inoue and Utada (1983)	This study	Fluid
T (°C)	250 ± 50°C	220°C	195°C
pH	4.5 ±0.5 at 25°C	4.6 at 220°C	7.0 at 195°C
Cl	0.89	0.99	0.84
Na	0.85	0.85	0.86
K	0.11	0.11	$3.6\ 10^{-10}$
Ca	$1.3\ 10^{-2}$	$1.3\ 10^{-2}$	$1.8\ 10^{-9}$
Mg	0.4 to $4.3\ 10^{-4}$	$4.3\ 10^{-4}$	$1.1\ 10^{-8}$
SO_4	$3.3\ 10^{-9}$	$3.3\ 10^{-9}$	$1.2\ 10^{-3}$
Al	--	$2.3\ 10^{-5}$	$5.0\ 10^{-3}$
Si	--	$6.5\ 10^{-3}$	195°C
C(4)	--	$7.8\ 10^{-4}$	--
Fe	--	--	$4.2\ 10^{-9}$
Smectite			30
Quartz			1
Gibbsite			1
Porosity			0.2

To our knowledge, smectite porewater has not been analysed. A hypothetical fluid composition was calculated (Table 3: Initial formation) assuming equilibrium with respect to pure smectite (composition given in Annex 1), quartz and gibbsite and considering the same Na concentration as that of the geothermal fluid.

Conceptual model

The modelling was based on a 1D column representing the vertical profile of the WS4 borehole. The profile consisted in 100 m of smectite, discretized into 100 cells of 1 m (see Figure 8). A linear temperature gradient from 220°C (inlet of the geothermal fluid) to 170°C (outlet of the geothermal fluid) was imposed, based on Inoue et al. (1992). A flowrate of 0.05 m year^{-1} was considered. The I/S compositions and thermodynamic properties are given in Annex 1. Geochemical calculations were performed using the code PhreeqC (Parkhurst and Appelo, 2013) and the thermodynamic database Thermoddem (Blanc et al., 2012), enriched with thermodynamic data established here (see Table A1 in Annex 1).

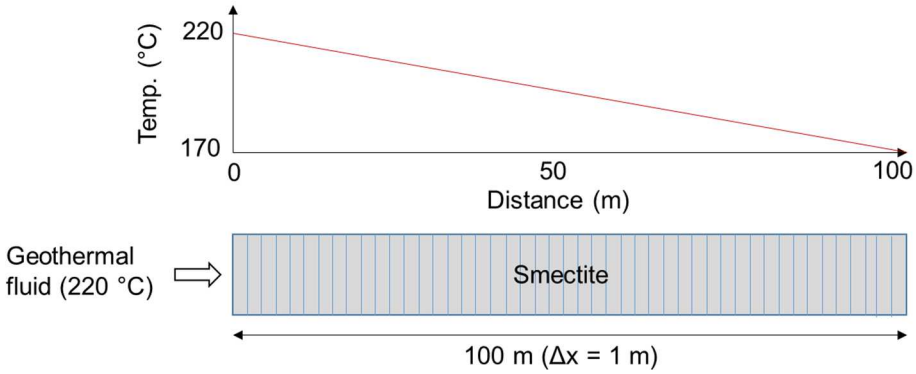

Figure 8 - *Discretized profile for the Shinzan WS4 borehole modelling.*

Results

Modelling results are reported in Figures 9, 10 and 11. Figure 9 shows the evolution of the smectite composition, revealing an efficient smectite-to-illite conversion up to the formation of an I/S with 80% illite after 10 Ma reaction time. As expected, the most relevant mineralogical transformation predicted by the numerical model is the pervasive illitization of the original rock, indicated by an augmented percentage of the illitic term in the I/S. The following sequence is obtained: from pure smectite to 10, 20, 30, 40, 50, 60, 70 and finally 80% illite after 10 Ma reaction time.

Another relevant feature of the mineralogical reworking predicted by the model is the concomitant precipitation of gibbsite and quartz. The occurrence of quartz (Figure 10) in our model is consistent with previous observations (Herman and Lahan, 1981) about the precipitation of quartz during the illitization of smectite, according to the scheme:

$$\text{smectite} + K^{+} \rightarrow \text{mixed-layer I/S} + \text{Quartz}$$

The porewater chemistry simulated after 10 Ma is shown in Figure 11. Contact with geothermal fluid led to acidic conditions between 0 and 10 m. The Si concentration decreased linearly from 0 to 100 m, consistent with the quartz equilibrium condition imposed under the fixed, linear temperature gradient of Figure 8. The Na concentration was constant during the entire simulation, and K concentrations remained quite unchanged over the first 100 m of the modelled domain (i.e. ~0.108 mol L^{-1}), in spite of the concomitant extensive illitization of the smectite fraction. The formation of illite-rich I/S phases was driven by high concentrations of aqueous Al.

Noteworthy, the smectite-to-illite transformation predicted by the model is consistent with the Miocene age of the formation documented by Inoue and Utada (1983). We consider the overall agreement between numerical results and field observations as an argument for the correctness of the thermodynamic properties predicted for the illite/smectite minerals of interest, and for the potential of our estimation tool. The geochemical model could be improved by including kinetically controlled reactions, like the Opal-A to Quartz transformation and potassium fixation, as a first step towards smectite illitization.

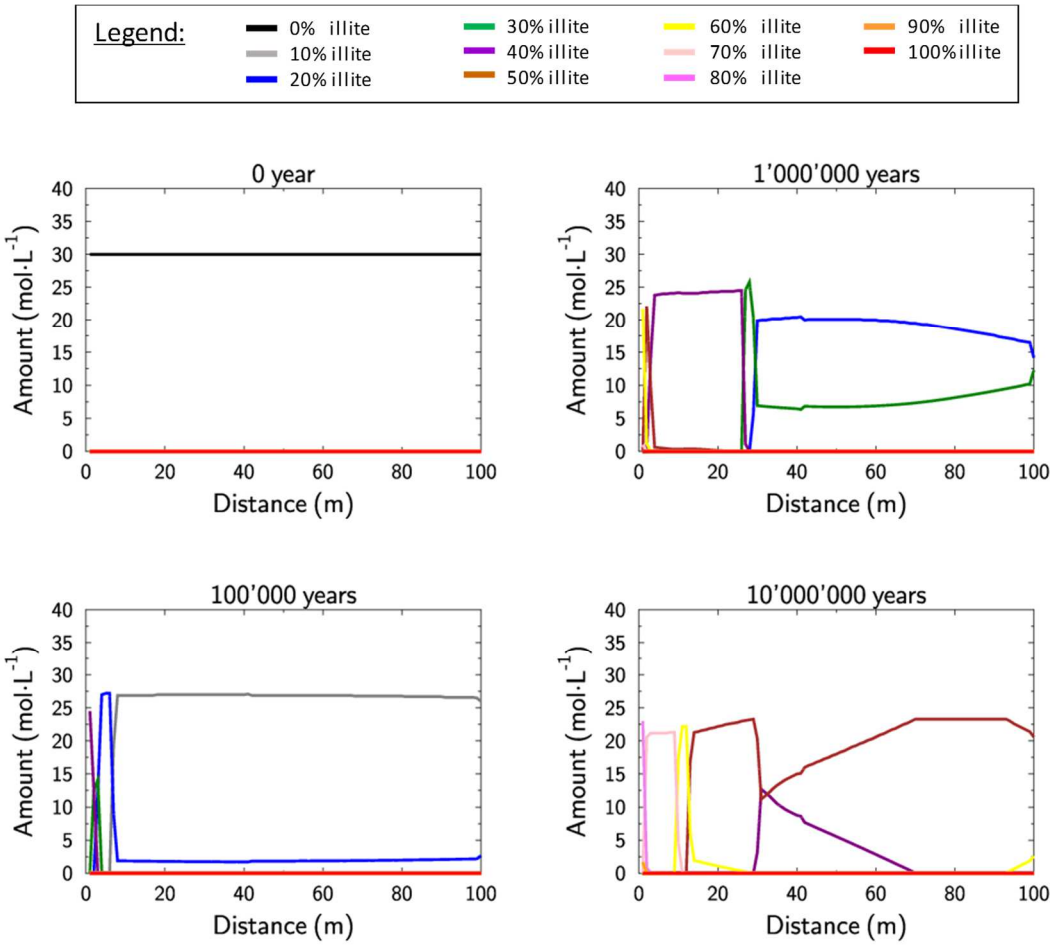

Figure 9 – *Modelling of the evolution of I/S composition during smectite hydrothermal transformation.*

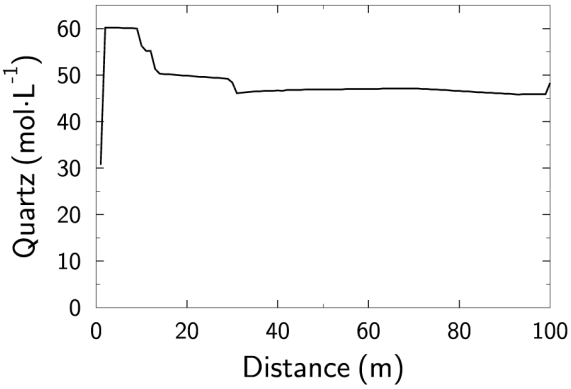

Figure 10 - *Modelled quartz profile after 10 Ma reaction time*

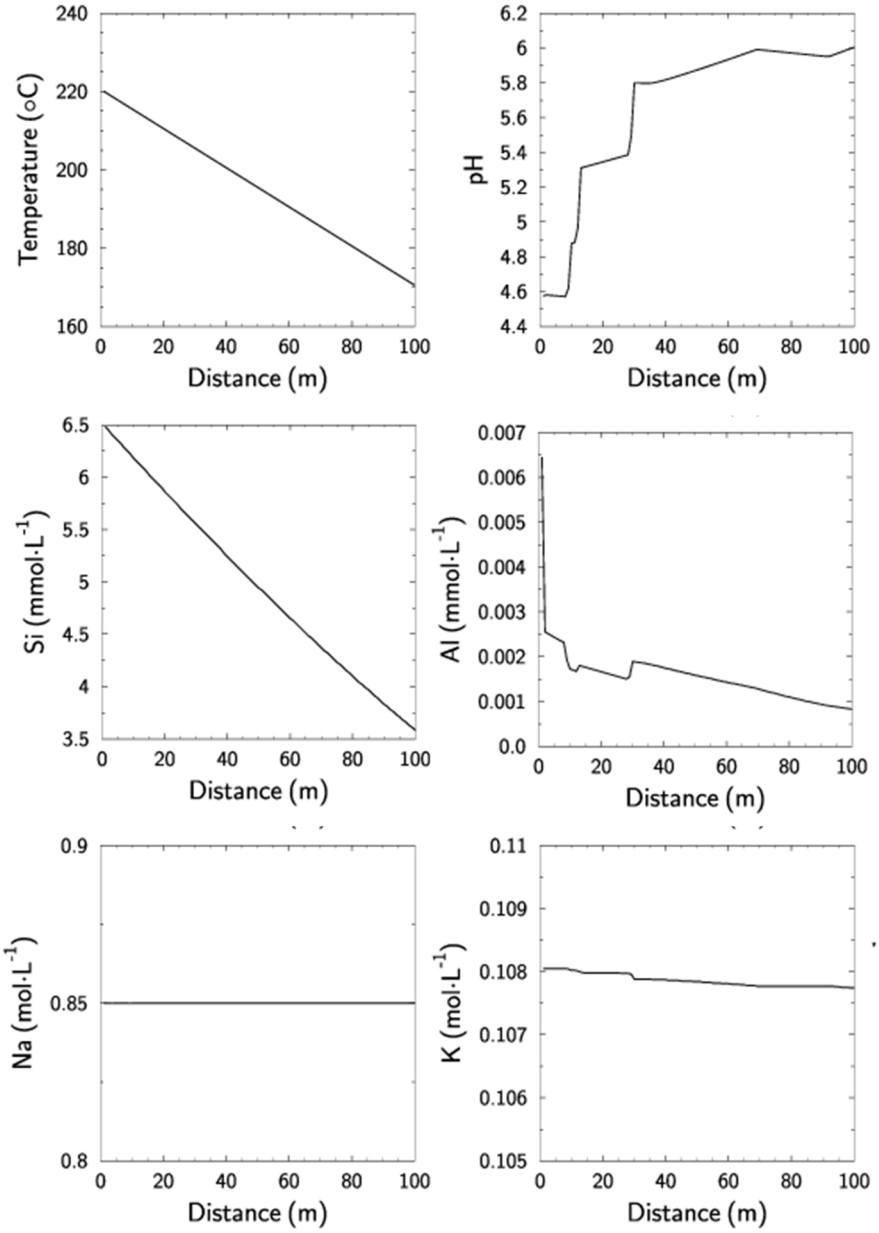

Figure 11 - *Porewater chemistry after 10 Ma reaction time*

6. Concluding remarks

We document the development of two calculation tools, ClayTherm and ISTherm, devoted to the estimation of the thermodynamic properties of clay minerals. These tools are aimed at combining pre-existing estimation models in new applications for their easy use in a potentially wider scientific community. Further to this, ClayTherm and ISTherm have the capability to model both anhydrous and hydrated phases more accurately than the models from which they derive.

The first estimation tool, ClayTherm, was developed by taking advantage of the estimation models previously fine-tuned by Blanc et al. (2015), Gailhanou et al. (2017) and Vieillard et al. (2019). Compared to these previous models, ClayTherm represents a refinement in the description of cation sharing among the crystallographic sites. The verification of the model was carried out by comparison of the numerical outputs with solubility data recently published by Gaboreau et al. (2020) and archived in the datasets selected by these authors from previous literature. ClayTherm estimations are in good agreement with data from the literature, calorimetry data included, except for chlorite, which was not found to reach equilibrium in solubility experiments. Some discrepancies between estimated and measured data were observed for vermiculite, possibly because of the presence of organic carbon in the sample measured by Gailhanou et al. (2013).

Directly derived from ClayTherm, the second estimation tool, ISTherm, is specifically designed to investigate the thermodynamic properties of interstratified illite/smectite minerals. In particular, it allows for the calculation of the thermodynamic properties of a series of illite/smectite (I/S) minerals from the composition of the smectitic and illitic end-members, and from a single I/S composition. The thermodynamic functions implemented in ISTherm, account for the specific contribution of the mixing energies term. The tool was used to investigate a natural I/S series from the Shinzan hydrothermal area, Japan. The results indicate that both temperature and hydration are first-order controlling parameters of the shape and extension of the illite/smectite stability fields. In particular, predominance stability fields of smectite-rich phases tend to increase when hydration is correctly accounted for in equilibrium reactions, whereas higher temperatures tend to displace the stability field of illite-rich phases towards higher activity values of dissolved silica.

The correctness of the estimated thermodynamic data was indirectly tested by a reactive transport modelling approach. Simplified, prototypical models were run to reproduce the hydrothermal alteration patterns observed in the Shinzan geothermal area, Japan. The formation of intermediate I/S phases during the illitization of smectite was successfully modelled, in agreement with site-specific mineralogical observations.

ACKNOWLEDGEMENTS

Financial support from the Thermochimie projects TemparSiamK (n° 20071653 CGK) and Domhyne (20081010 COX) and from the Stab-Inter BRGM/IGG project are gratefully acknowledged. Exchanges and contributions from Arnault Lassin, Mathieu Debure and Francis Claret at BRGM and Claire Fialips from Total were particularly helpful to us and welcomed. The whole project could not be completed without the contributions of colleagues from Marseille (IM2NP: Jacques Rogez and Georges Mikaelian, MADIREL: Renaud Denoyel and Emily Bloch) and from Tokyo (TOKYOTECH: Hitoshi Kawaji), we are very grateful to them. This article is especially dedicated to the late Eric Giffaut, whose talent and constant efforts were decisive in achieving this 17-year suite of scientific programs.

7. References

Aagaard, P., Helgeson, H.C., 1983. Activity/composition relations among silicates and aqueous solutions: II. Chemical and thermodynamic consequences of ideal mixing of atoms on homological sites in montmorillonites, illites, and mixed-layer clays. Clays and Clay Minerals 31, 207-217.

Aja, S.U., Rosenberg, P.E., Kittrick, J.A., 1991. Illite equilibria in solutions: I. Phase relationships in the system K_2O-Al_2O_3-SiO_2-H_2O between 25 and 250°C. Geochimica et Cosmochimica Acta 55, 1353-1364.

Amouric, M., Olives, J., 1991. Illitization of smectite as seen by high-resolution transmission electron microscopy. European Journal of Mineralogy 3, 831-835.

Battaglia, S., Gherardi, F., Gianelli, G., Leoni, L., Lezzerini, M., 2013. Alteration of clay minerals in a sedimentary caprock and its use in geothermal prospecting: an example from Mt. Amiata. Clay Minerals 48, 37-58.

Benson, S.W., 1968. Thermochemical kinetics: methods for the estimation of thermochemical data and rate parameters. Wiley.

Bertoldi, C., Dachs, E., Cemic, L., Theye, T., Wirth, R., Groger, W., 2005. The heat capacity of the serpentine subgroup mineral berthierine $(Fe_{2.5}Al_{0.5})[Si_{1.5}Al_{0.5}O_5](OH)_4$. Clays and Clay Minerals 53, 380-388.

Blanc, P., Bieber, A., Fritz, B., Duplay, J., 1997. A short range interaction model applied to illite/smectite mixed-layer minerals. Physics and Chemistry of Minerals 24, 574-581.

Blanc, P., Gailhanou, H., Rogez, J., Mikaelian, G., Kawaji, H., Warmont, F., Gaboreau, S., Grangeon, S., Grenèche, J.-M., Vieillard, P., Fialips, C.I., Giffaut, E., Gaucher, E.C., Claret, F., 2014. Thermodynamic properties of chlorite and berthierine derived from calorimetric measurements. Physics and Chemistry of Minerals 41, 603-615.

Blanc, P., Lassin, A., Piantone, P., Azaroual, M., Jacquemet, N., Fabbri, A., Gaucher, E.C., 2012. Thermoddem: A geochemical database focused on low temperature water/rock interactions and waste materials. Applied Geochemistry 27, 2107-2116.

Blanc, P., Vieillard, P., Gailhanou, H., Gaboreau, S., Gaucher, E.C., Fialips, C.I., Madé, B., Giffaut, E., 2015. A generalized model for predicting the thermodynamic properties of clay minerals. American Journal of Science 315, 734-780.

Brown, G., 1982. Crystal structures of clay minerals and their X-ray identification. The Mineralogical Society of Great Britain and Ireland.

Chermak, J.A., Rimstidt, J.D., 1989. Estimating the thermodynamic properties ($\Delta G°f$ and $\Delta H°f$) of silicate minerals at 298 K from the sum of polyhedral contributions. American Mineralogist 74, 1023-1031.

Circone, S., Navrotsky, A., 1992. Substitution of $^{[6,4]}$Al in phlogopite; high-temperature solution calorimetry, heat capacities, and thermodynamic properties of the phlogopite-eastonite join. American Mineralogist 77, 1191-1205.

Compton, J.S., 1991. Origin and diagenesis of clay minerals in the Monterey Formation, Santa Maria Basin Area, California. Clays and Clay Minerals 39, 449-466.

Coudrain-Ribstein, A., Gouze, P., de Marsily, G., 1998. Temperature-carbon dioxide partial pressure trends in confined aquifers. Chemical Geology 145, 73-89.

Cox, J.D., Wagman, D.D., Medvedev, V.A., 1989. CODATA key values for thermodynamics. Hemisphere Pub. Corp.

Dachs, E., Benisek, A., 2019. A new activity model for Mg–Al biotites determined through an integrated approach. Contributions to Mineralogy and Petrology 174, 76.

Dubacq, B., Vidal, O., Andrade, V.D., 2010. Dehydration of dioctahedral aluminous phyllosilicates: thermodynamic modelling and implications for thermobarometric estimates. Contributions to Mineralogy and Petrology 159, 159-174.

Essene, E.J., Peacor, D.R., 1995. Clay mineral thermometry; a critical perspective. Clays and Clay Minerals 43, 540-553.

Gaboreau, S., Gailhanou, H., Blanc, P., Vieillard, P., Made, B., 2020. Clay mineral solubility from aqueous equilibrium: Assessment of the measured thermodynamic properties. Applied Geochemistry 113, 104465.

Gailhanou, H., 2005. Détermination expérimentale des propriétés thermodynamiques et étude des nanostructures de minéraux argileux. Aix-Marseille 3, p. 262.

Gailhanou, H., Blanc, P., Rogez, J., Mikaelian, G., Horiuchi, K., Yamamura, Y., Saito, K., Kawaji, H., Warmont, F., Grenèche, J.-M., Vieillard, P., Fialips, C.I., Giffaut, E., Gaucher, E.C., 2013. Thermodynamic properties of saponite, nontronite, and vermiculite derived from calorimetric measurements. American Mineralogist 98, 1834-1847.

Gailhanou, H., Blanc, P., Rogez, J., Mikaelian, G., Kawaji, H., Olives, J., Amouric, M., Denoyel, R., S., B., Montouillout, V., Vieillard, P., Fialips, C.I., Giffaut, E., Michau, N., Gaucher, E.C., 2012. Thermodynamic properties of illite IMt-2, smectite MX-80 and beidellite SBld-1 by calorimetric methods: Enthalpies of formation, heat capacities , entropies and Gibbs free energies of formation. Geochimica Cosmochimica Acta 89, 279-301.

Gailhanou, H., Blanc, P., Rogez, J., Mikaelian, G., Kawaji, H., Olives, J., Montouillout, V., Grenèche, J.M., Vieillard, P., Gaucher, E.C., Fialips, C.I., Madé, B., 2019. Thermodynamic properties of mixed-layer illite-smectite by calorimetric methods: Acquisition of the enthalpies of mixing of illite and smectite layers. The Journal of Chemical Thermodynamics 138, 78-97.

Gailhanou, H., Rogez, J., Miltenburg, J.C.v., Genderen, A.C.G.v., Grenèche, J.M., Gilles, C., Jalabert, D., Michau, N., Gaucher, E.C., Blanc, P., 2009. Thermodynamic properties of chlorite CCa-2. Heat capacities, heat contents and entropies. Geochimica et Cosmochimica Acta 73, 4738-4749.

Gailhanou, H., van Miltenburg, J.C., Rogez, J., Olives, J., Amouric, M., Gaucher, E.C., Blanc, P., 2007. Thermodynamic properties of anhydrous smectite MX-80, illite IMt-2 and mixed-layer illite–smectite ISCz-1 as determined by calorimetric methods. Part I: Heat capacities, heat contents and entropies. Geochimica et Cosmochimica Acta 71, 5463-5473.

Gailhanou, H., Vieillard, P., Blanc, P., Lassin, A., Denoyel, R., Bloch, E., De Weireld, G., Gaboreau, S., Fialips, C.I., Madé, B., Giffaut, E., 2017. Methodology for determining the thermodynamic properties of smectite hydration. Applied Geochemistry 82, 146-163.

Garrels, R.M., 1984. Montmorillonite/illite stability diagrams. Clays and Clay minerals 32, 161-166.

Gaucher, E.C., Tournassat, C., Pearson, F.J., Blanc, P., Crouzet, C., Lerouge, C., Altmann, S., 2009. A robust model for pore-water chemistry of clayrock. Geochimica et Cosmochimica Acta 73, 6470-6487.

Geloni, C., Previde Massara, E., Di Paola, E., Ortenzi, A., Blanc, P., Gherardi, F., 2017. Modelling clay diagenesis using a combined crystal chemistry and thermochemistry approach: a case study on smectite illitization. Energy Procedia 125, 630-639.

Gherardi, F., Audigane, P., 2014. Geochemical reactivity in CO_2 geological storage sites. Greenhouse Gas Sci Technol 4, 157-159.

Giffaut, E., Grivé, M., Blanc, P., Vieillard, P., Colàs, E., Gailhanou, H., Gaboreau, S., Marty, N., Madé, B., Duro, L., 2014. ANDRA thermodynamic database for performance assessment: ThermoChimie. Applied Geochemistry 49, 225-236.

Helgeson, H., Delany, J., Nesbitt, H., Bird, D., 1978. Summary and critique of the thermodynamic properties of rock-forming minerals. American Journal of Science 278, 1-229.

Hemingway, B.S., Robie, R.A., Kittrick, J.A., Grew, E.S., Nelen, J.A., London, D., 1984. The heat capacities of osumilite from 298.15 to 1000 K, the thermodynamic properties of two natural chlorites to 500 K, and the thermodynamic properties of petalite to 1800 K. United States Geological Survey, pp. 701-710.

Herman, R.E., Lahan, R.W., 1981. Smectite to illite conversion rates: effects of solution chemistry. Clays and Clay Minerals 29, 129-135.

Holland, T.J.B., 1989. Dependance of entropy on volume for silicate and oxide minerals. A review and a prediction model. American Mineralogist, 74, 5-13.

Holland, T.J.B., Powell, R., 1998. An internally consistent thermodynamic data set for phases of petrological interest. Journal of Metamorphic Geology 16, 309-343.

Hower, J., Mowatt, T.C., 1966. The mineralogy of illites and mixed-layer illite/ montmorillonites. American Mineralogist 51, 825-854.

Huang, W.H., Keller, W.D., 1973. Gibbs free energy of formation calculated from dissolution data using specific mineral analyses. American Mineralogist 58, 1023-1028.

Inoue, A., 1983. Potassium fixation by clay minerals during hydrothermal treatment. Clays and Clay Minerals 31, 81-91.

Inoue, A., Kohyama, N., Kitagawa, R., Watanabe, T., 1987. Chemical and morphological evidence for the conversion of smectite to illite. Clays and Clay Minerals 35, 111-120.

Inoue, A., Utada, M., 1983. Further Investigations of a conversion series of dioctahedral mica/smectites in the Shinzan hydrothermal alteration area, northeast Japan. Clays and Clay Minerals 31, 401-412.

Inoue, A., Utada, M., Wakita, K., 1992. Smectite-to-illite conversion in natural hydrothermal systems. Applied Clay Science 7, 131-145.

Kittrick, J.A., 1984. Solubility measurements of phases in three illites. Clays and Clay Minerals 32, 115-124.

Kittrick, J.A., Peryea, F.J., 1988. Experimental validation of the monophase structure model for montmorillonite solubility. Soil Science Society of America Journal 52, 1199-1201.

Landais, P., 2006. Advances in geochemical research for the underground disposal of high-level, long-lived radioactive waste in a clay formation. Journal of Geochemical Exploration 88, 32-36.

Marty, N.C.M., Tournassat, C., Burnol, A., Giffaut, E., Gaucher, E.C., 2009. Influence of reaction kinetics and mesh refinement on the numerical modelling of concrete/clay interactions. Journal of Hydrology 364, 58-72.

May, H.M., Klnniburgh, D.G., Helmke, P.A., Jackson, M.L., 1986. Aqueous dissolution, solubilities and thermodynamic stabilities of common aluminosilicate clay minerals: Kaolinite and smectites. Geochimica et Cosmochimica Acta 50, 1667-1677.

Meunier, A., Lanson, B., Velde, B., 2004. Composition variation of illite-vermiculite-smectite mixed-layer minerals in a bentonite bed from Charente (France). Clay Minerals 39, 317-332.

Meunier, A., Velde, B., 1989. Solid solutions in I/S mixed-layer minerals and illite. American Mineralogist 74, 1106-1112.

Meunier, A., Velde, B., Griffault, L., 1998. The reactivity of bentonites: A review. An application to clay barrier stability for nuclear waste storage. Clay Minerals 33, 187-196.

Misra, U., Upchurch, W., 1976. Free energy of formation of beidellite from apparent solubility measurements. Clays and Clay Minerals 24, 327-331.

Olives, J., Amouric, M., Perbost, R., 2000. Mixed layering of illite-smectite: Results from high-resolution transmission electron microscopy and lattice-energy calculations. Clays and Clay Minerals 48, 282-289.

Parkhurst, D.L., Appelo, C., 2013. Description of input and examples for PHREEQC version 3: A computer program for speciation, batch-reaction, one-dimensional transport, and inverse geochemical calculations. US Geological Survey.

Reesman, A.L., Keller, W.D., 1968. Aqueous solubility of high alumina and clay minerals. American Mineralogist 53, 929-941.

Tremosa, J., Gailhanou, H., Chiaberge, C., Castilla, R., Gaucher, E.C., Lassin, A., Gout, C., Fialips, C., Claret, F., 2020. Effects of smectite dehydration and illitisation on overpressures in sedimentary basins: A coupled chemical and thermo-hydro-mechanical modelling approach. Marine and Petroleum Geology 111, 166-178.

Ulbrich, H.H., Waldbaum, D.R., 1976. Structural and other contributions to the third-law entropies of silicates. Geochimica et Cosmochimica Acta 40, 1-24.

Van Hinsberg, V.J., Vriend, S.P., Schumacher, J.C., 2005a. A new method to calculate end-member thermodynamic properties of minerals from their constituent polyhedra I: enthalpy, entropy and molar volume. Journal of Metamorphic Geology 23, 165-179.

Van Hinsberg, V.J., Vriend, S.P., Schumacher, J.C., 2005b. A new method to calculate end-member thermodynamic properties of minerals from their constituent polyhedra II: heat capacity, compressibility and thermal expansion. Journal of Metamorphic Geology 23, 681-693.

Velde, B., 1992. The stability of clays, in: Price, G.D., Ross, N.L. (Eds.), The Stability of Minerals. Springer Netherlands, Dordrecht, pp. 329-351.

Velde, B., Vasseur, G., 1992. Estimation of the diagenetic smectite to illite transformation in time-temperature space. American Mineralogist 77, 967-976.

Vidal, O., Dubacq, B., 2009. Thermodynamic modelling of clay dehydration, stability and compositional evolution with temperature, pressure and H_2O activity. Geochimica et Cosmochimica Acta 73, 6544-6564.

Vieillard, P., 1994a. Prediction of enthalpy of formation based on refined crystal structures of multisite compounds: Part 1. Theories and examples. Geochimica et Cosmochimica Acta 58, 4049-4063.

Vieillard, P., 1994b. Prediction of enthalpy of formation based on refined crystal structures of multisite compounds: Part 2. Application to minerals belonging to the system Li_2O-Na_2O-K_2O-BeO-MgO-CaO-MnO-FeO-Fe_2O_3-Al_2O_3-SiO_2-H_2O. Results and discussion. Geochimica et Cosmochimica Acta 58, 4065-4107.

Vieillard, P., 2000. A new method for the prediction of Gibbs free energies of formation of hydrated clay minerals based on the electronegativity scale. Clays and Clay Minerals 48, 459-473.

Vieillard, P., 2002. A new method for the prediction of Gibbs free energies of formation of phyllosilicates (10 Å and 14 Å) based on the electronegativity scale. Clays and Clay Minerals 50, 352-363.

Vieillard, P., Gailhanou, H., Lassin, A., Blanc, P., Bloch, E., Denoyel, R., Gaboreau, S., Fialips, C.I., Made, B., 2019. A predictive model of thermodynamic entities of hydration for smectites: application to the formation properties of smectites. Applied Geochemistry 110, 104423.

Vieillard, P., Tardy, Y., 1988. Estimation of enthalpies of formation of minerals based on their refined crystal structures. American Journal of Science 288, 997-1040.

Vinograd, V.L., 1995. Substitution of $^{[4]}Al$ in layer silicates: Calculation of the Al-Si configurational entropy according to ^{29}Si NMR Spectra. Physics and Chemistry of Minerals 22, 87-98.

Wertz, F., Gherardi, F., Blanc, P., Bader, A.-G., Fabbri, A., 2013. Cement CO_2-alteration propagation at the well–caprock–reservoir interface and influence of diffusion. International Journal of Greenhouse Gas Control 12, 9-17.

Yamada, H., Yoshioka, K., Tamura, K., Fujii, K., Nakazawa, H., 1999. Compositional gap in dioctahedral-trioctahedral smectite system: beidellite-saponite pseudo-binary join. Clays and Clay Minerals 47, 803-810.

Annex 1 – I/S mineral compositions and thermodynamic properties calculated for the WS4 Shinzan series

Table A1 - I/S compositions and thermodynamic properties calculated using ISTherm, for the WS4 Shinzan series.

Formula	% illite	ΔH^0_f kJ.mol^{-1}	S^0 J.mol^{-1}.K^{-1}	C^0_p J.mol^{-1}.K^{-1}	V^0 cm^3.mol^{-1}
Sample B from Gailhanou (2005) and Gailhanou et al. (2019) (1) $(K_{0.15}Na_{0.23}Ca_{0.06})(Mg_{0.4}Fe^{II}_{0.04}Al_{1.49}Fe^{III}_{0.11})(Si_{3.82}Al_{0.18})O_{10}(OH)_2$	15				
Anhydrous minerals					
$(K_{0.014}Na_{0.275}Ca_{0.072})(Mg_{0.437}Fe_{0.164}Al_{1.439})(Si_{3.925}Al_{0.075})O_{10}(OH)_2$	0	-5641.05	297.99	314.45	135.97
$(K_{0.098}Na_{0.248}Ca_{0.065})(Mg_{0.414}Fe_{0.156}Al_{1.47})(Si_{3.861}Al_{0.139})O_{10}(OH)_2$	10	-5665.14	301.93	315.81	136.37
$(K_{0.181}Na_{0.22}Ca_{0.058})(Mg_{0.392}Fe_{0.147}Al_{1.501})(Si_{3.796}Al_{0.204})O_{10}(OH)_2$	20	-5689.33	304.63	317.16	136.77
$(K_{0.265}Na_{0.193}Ca_{0.05})(Mg_{0.369}Fe_{0.139}Al_{1.532})(Si_{3.732}Al_{0.268})O_{10}(OH)_2$	30	-5713.46	306.79	318.52	137.17
$(K_{0.348}Na_{0.165}Ca_{0.043})(Mg_{0.347}Fe_{0.13}Al_{1.563})(Si_{3.667}Al_{0.333})O_{10}(OH)_2$	40	-5737.41	308.55	319.88	137.57
$(K_{0.432}Na_{0.138}Ca_{0.036})(Mg_{0.324}Fe_{0.122}Al_{1.595})(Si_{3.603}Al_{0.397})O_{10}(OH)_2$	50	-5761.05	309.96	321.23	137.97
$(K_{0.516}Na_{0.11}Ca_{0.029})(Mg_{0.301}Fe_{0.113}Al_{1.626})(Si_{3.538}Al_{0.462})O_{10}(OH)_2$	60	-5784.27	311.03	322.59	138.37
$(K_{0.599}Na_{0.083}Ca_{0.022})(Mg_{0.279}Fe_{0.104}Al_{1.657})(Si_{3.474}Al_{0.526})O_{10}(OH)_2$	70	-5807.01	311.75	323.94	138.77
$(K_{0.683}Na_{0.055}Ca_{0.014})(Mg_{0.256}Fe_{0.096}Al_{1.688})(Si_{3.409}Al_{0.591})O_{10}(OH)_2$	80	-5829.19	312.08	325.30	139.17
$(K_{0.766}Na_{0.027}Ca_{0.007})(Mg_{0.234}Fe_{0.087}Al_{1.719})(Si_{3.345}Al_{0.655})O_{10}(OH)_2$	90	-5850.76	311.86	326.66	139.56
$(K_{0.85})(Mg_{0.211}Fe_{0.079}Al_{1.75})(Si_{3.28}Al_{0.72})O_{10}(OH)_2$	100	-5871.70	310.40	328.01	139.96
Hydrated minerals					
$(K_{0.014}Na_{0.275}Ca_{0.072})(Mg_{0.437}Fe_{0.164}Al_{1.439})(Si_{3.925}Al_{0.075})O_{10}(OH)_2 \cdot 3.23H_2O$	0	-6583.86	484.94	557.12	194.34
$(K_{0.098}Na_{0.248}Ca_{0.065})(Mg_{0.414}Fe_{0.156}Al_{1.47})(Si_{3.861}Al_{0.139})O_{10}(OH)_2 \cdot 2.91H_2O$	10	-6513.67	470.19	534.21	188.90
$(K_{0.181}Na_{0.22}Ca_{0.058})(Mg_{0.392}Fe_{0.147}Al_{1.501})(Si_{3.796}Al_{0.204})O_{10}(OH)_2 \cdot 2.58H_2O$	20	-6443.58	454.20	511.30	183.46
$(K_{0.265}Na_{0.193}Ca_{0.05})(Mg_{0.369}Fe_{0.139}Al_{1.532})(Si_{3.732}Al_{0.268})O_{10}(OH)_2 \cdot 2.26H_2O$	30	-6373.43	437.66	488.39	178.03
$(K_{0.348}Na_{0.165}Ca_{0.043})(Mg_{0.347}Fe_{0.13}Al_{1.563})(Si_{3.667}Al_{0.333})O_{10}(OH)_2 \cdot 1.94H_2O$	40	-6303.09	420.72	465.48	172.59
$(K_{0.432}Na_{0.138}Ca_{0.036})(Mg_{0.324}Fe_{0.122}Al_{1.595})(Si_{3.603}Al_{0.397})O_{10}(OH)_2 \cdot 1.62H_2O$	50	-6232.45	403.44	442.57	167.15
$(K_{0.516}Na_{0.11}Ca_{0.029})(Mg_{0.301}Fe_{0.113}Al_{1.626})(Si_{3.538}Al_{0.462})O_{10}(OH)_2 \cdot 1.29H_2O$	60	-6161.40	385.81	419.66	161.71
$(K_{0.599}Na_{0.083}Ca_{0.022})(Mg_{0.279}Fe_{0.104}Al_{1.657})(Si_{3.474}Al_{0.526})O_{10}(OH)_2 \cdot 0.97H_2O$	70	-6089.85	367.84	396.75	156.28
$(K_{0.683}Na_{0.055}Ca_{0.014})(Mg_{0.256}Fe_{0.096}Al_{1.688})(Si_{3.409}Al_{0.591})O_{10}(OH)_2 \cdot 0.65H_2O$	80	-6017.75	349.47	373.83	150.84
$(K_{0.766}Na_{0.027}Ca_{0.007})(Mg_{0.234}Fe_{0.087}Al_{1.719})(Si_{3.345}Al_{0.655})O_{10}(OH)_2 \cdot 0.32H_2O$	90	-5945.04	330.56	350.92	145.40

(1) Ti (0.006 cations per $O_{10}(OH)_2$, in original B sample) is replaced by Al, for sake of simplicity.

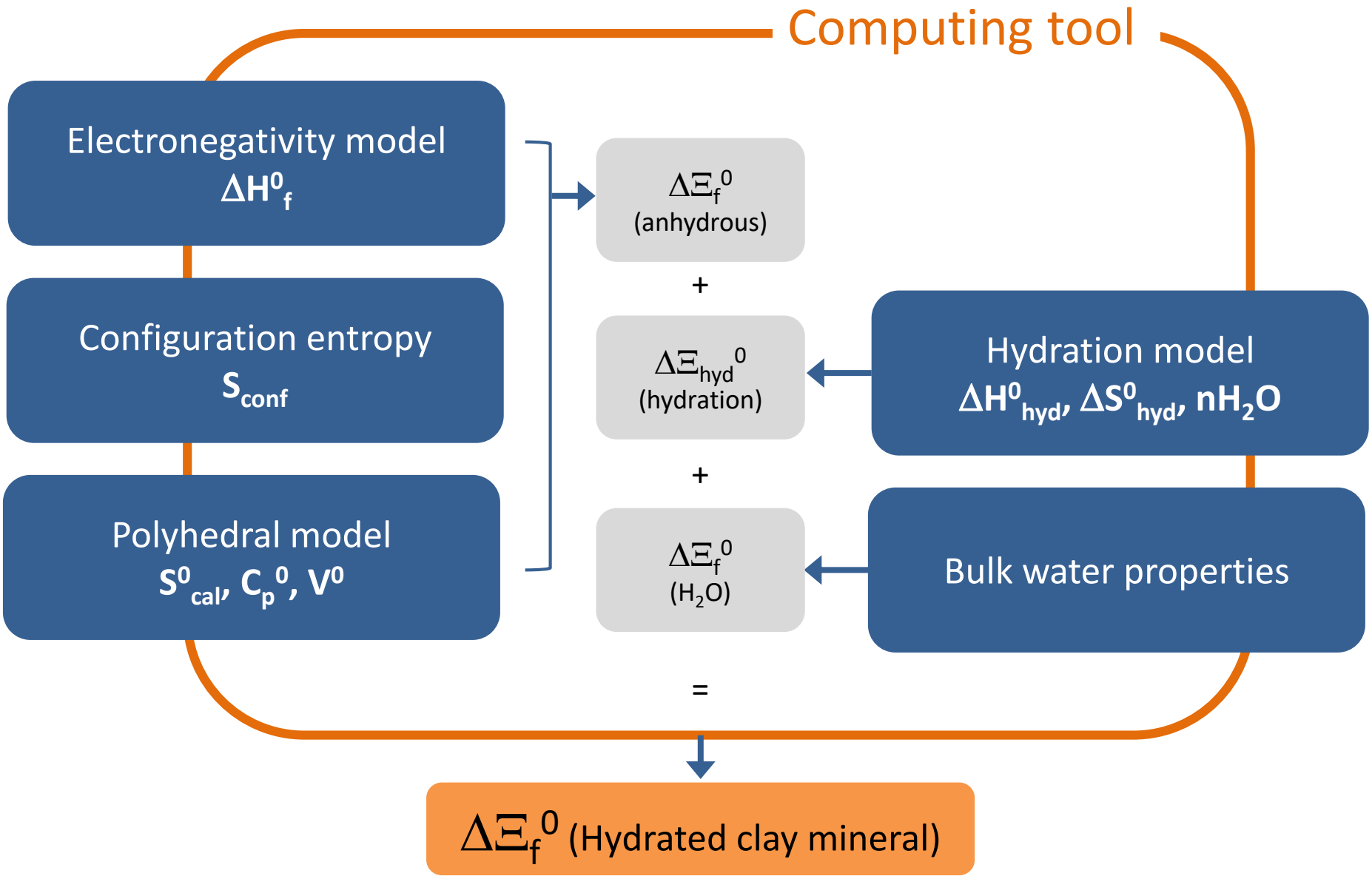
Computing tool
Electronegativity model
ΔH^0_f
Configuration entropy
S_{conf}
Polyhedral model
S^0_{cal}, $C_p{}^0$, V^0
$\Delta \Xi_f{}^0$ (anhydrous)
+
$\Delta \Xi_{hyd}{}^0$ (hydration)
+
$\Delta \Xi_f{}^0$ (H_2O)
=
Hydration model
ΔH^0_{hyd}, ΔS^0_{hyd}, nH_2O
Bulk water properties
$\Delta \Xi_f{}^0$ (Hydrated clay mineral)